



Enhanced Performance of Perovskite Single-Crystal Photodiodes by Epitaxial Hole Blocking Layer

Yuzhu Pan¹, Xin Wang^{1*}, Yubing Xu¹, Yuwei Li¹, Elias Emeka Elemike², Ahmed Shuja³, Qing Li¹, Xiaobing Zhang¹, Jing Chen¹, Zhiwei Zhao¹ and Wei Lei^{1*}

¹ School of Electronic Science and Engineering, Joint International Research Laboratory of Information Display and Visualization, Southeast University, Nanjing, China, ² Chemistry Department of North West University, Mafikeng, South Africa, ³ Centre for Advanced Electronics and Photovoltaic Engineering, International Islamic University, Islamabad, Pakistan

OPEN ACCESS

Edited by:

Zhaolai Chen,
Shandong University, China

Reviewed by:

Andrew Nattestad,
University of Wollongong, Australia
Liang Shen,
Jilin University, China

*Correspondence:

Xin Wang
230159424@seu.edu.cn
Wei Lei
lw@seu.edu.cn

Specialty section:

This article was submitted to
Inorganic Chemistry,
a section of the journal
Frontiers in Chemistry

Received: 30 March 2020

Accepted: 28 July 2020

Published: 10 September 2020

Citation:

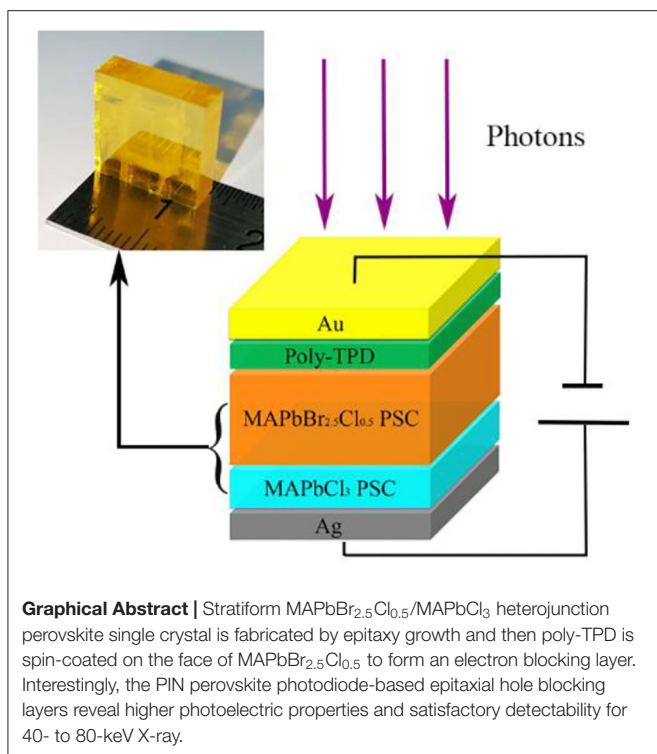
Pan Y, Wang X, Xu Y, Li Y, Elemike EE, Shuja A, Li Q, Zhang X, Chen J, Zhao Z and Lei W (2020) Enhanced Performance of Perovskite Single-Crystal Photodiodes by Epitaxial Hole Blocking Layer. *Front. Chem.* 8:791. doi: 10.3389/fchem.2020.00791

Introducing hole/electron transporting and blocking layers is considered to enhance the performance of electronic devices based on organic–inorganic hybrid halide perovskite single crystals (PSCs). In many photodiodes, the hole/electron transporting or blocking materials are spin-coated or thermal-evaporated on PSC to fabricate heterojunctions. However, the heterojunction interfaces due to lattice mismatch between hole/electron, transporting or blocking materials and perovskites easily form traps and cracks, which cause noise and leakage current. Besides, these low-mobility transporting layers increase the difficulty of transporting carriers generated by photons to the electrode; hence, they also increase the response time for photo detection. In the present study, MAPbCl₃-MAPbBr_{2.5}Cl_{0.5} heterojunction interfaces were realized by liquid-phase epitaxy, in which MAPbBr_{2.5}Cl_{0.5} PSC acts as an active layer and MAPbCl₃ PSC acts as a hole blocking layer (HBL). Our PIN photodiodes with epitaxial MAPbCl₃ PSC as HBL show better performance in dark current, light responsivity, stability, and response time than the photodiodes with spin-coated organic PCBM as HBL. These results suggest that the heterojunction interface formed between two bulk PSCs with different halide compositions by epitaxy growth is very useful for effectively blocking the injected charges under high external electric field, which could improve the collection of photo-generated carriers and hereby enhance the detection performance of the photodiode. Furthermore, the PIN photodiodes made of PSC with epitaxial HBL show the sensitivities of 7.08 mC Gy_{air}⁻¹ cm⁻², 4.04 mC Gy_{air}⁻¹ cm⁻², and 2.38 mC Gy_{air}⁻¹ cm⁻² for 40-keV, 60-keV, and 80-keV X-ray, respectively.

Keywords: perovskite single crystals, heterojunction, PIN diodes, epitaxial growth, photoelectric detection

INTRODUCTION

Perovskite is a promising candidate among new-generation opto-electronic material for applications in solar cells and light-emitting diodes owing to its outstanding optical and electrical characteristics (Kojima et al., 2009; Tan et al., 2014; Ju et al., 2018). In particular, organic–inorganic hybrid halide lead single crystal perovskites (MAPbX₃, where MA = CH₃NH₃ and X = Cl, Br, or I) with high atomic numbers have been studied. Excellent carrier mobility, low trap density, long carrier diffusion length, and high absorption coefficient indicate that they could be applied



not only in regular ultraviolet, visible, and near-infrared light, but also in X-ray and gamma-ray detection and imaging (Wang et al., 2015; Yakunin et al., 2015; Wei et al., 2016; Gill et al., 2018). For perovskite photodiodes, the vertical (sandwich-like) topology structures generated by introducing hole/electron transporting or blocking layers are considered to enhance the performance (Wang and Kim, 2017; Zeng et al., 2017). In many devices based on perovskite crystal, n-type materials including fullerene-derivative phenyl-C61-butyric acid methyl ester (PCBM), ZnO, and TiO₂ act both as electron transport layers (ETL) and hole blocking layers (HBL). The p-type polymers including poly[N,N'-bis(4-butylphenyl)-N,N'-bis(phenyl)-benzidine] (poly-TPD), poly(ethylenedioxythiophene):polystyrene sulfonate (PEDOT:PSS), poly(9-vinylcarbazole) (PVK), and poly[bis(4-phenyl)(2,4,6-trimethylphenyl)amine] (PTAA) are used both as hole transport layers (HTLs) and electron blocking layers (EBLs) (Dai et al., 2014; Jara et al., 2014; Liu and Kelly, 2014; Malinkiewicz et al., 2014).

The intimate contact between the active layer and hole/electron blocking layers is essential for blocking injected charges and effectively collecting carriers to the electrodes (Chen et al., 2017; Cheng et al., 2019). However, these additional layered transporting and blocking layers deposited by spin-coating or thermal evaporation have a low mobility lifetime and high trap density because these layers are amorphous and have lattice mismatch on PSC interfaces (Lin et al., 2015; Zhang et al., 2017). In addition, surface traps or cracks are easily formed when they deposit large-area and 10-nm-thick functional layers that would cause large noise and leaking current (Fang and

Huang, 2015; Wang et al., 2019). MAPbBr_{2.5}Cl_{0.5} PSC has been proven to possess large resistivity, high mobility, and low degree of lattice mismatch as compared to MAPbCl₃ PSC (Sutherland and Sargent, 2016; Jiang et al., 2019; Ou et al., 2019). Therefore, it is feasible to fabricate lattice-matched heterojunctions with the energy band gradient between MAPbBr_{2.5}Cl_{0.5} PSC and MAPbCl₃ PSC by epitaxy growth. This would significantly decrease the leaking current and accelerate carrier transport, leading to a high-performance PSC photodetector (Li et al., 2019b).

This article demonstrates a facile process for fabricating stratiform MAPbBr_{2.5}Cl_{0.5}/MAPbCl₃ heterojunction PSCs by liquid-phase epitaxial growth. MAPbBr_{2.5}Cl_{0.5} PSC mainly acts as an active layer to absorb photons and n-type MAPbCl₃ PSC as HBL to decrease the positive charges injected from the anode. Subsequently, p-type organic molecules poly-TPD are deposited on the opposite faces of doped MAPbBr_{2.5}Cl_{0.5} PSC to form HTL to block the negative charges injected from the cathode. Finally, the gold and silver films are deposited on the faces of poly-TPD and MAPbCl₃ PSC as anode and cathode, respectively. The device with electron transport material PCBM and C60 as HBL was fabricated by spin coating to compare with our device. Our PIN photodiode supplanted organic micro molecule with MAPbCl₃ PSC acting as HBL on MAPbBr_{2.5}Cl_{0.5} PSC shows a lower dark current density, greater responsivity, and faster response time. It demonstrates the superiority of taking lattice matched heterojunction by epitaxy growth in the fabricating of perovskite diode. Furthermore, the PIN photodiode with epitaxial MAPbCl₃ PSC as HBL also shows excellent performance on low-energy X-ray detection due to it being a few millimeters in thickness.

MATERIALS AND METHODS

Materials

Methylamine ethanol solution (CH₃NH₂, 33 wt.%), hydrobromic acid (HBr, 48 wt.%), hydrochloric acid (HCl, 37 wt.%), poly-TPD, PCBM, and C60 (99.99%) were obtained from Aladdin. N,N-Dimethylformamide (DMF) and dimethyl sulfoxide (DMSO) were obtained from Alfa Aesar. Lead chloride (PbCl₂, 99.9%) and lead bromide (PbBr₂, 99.9%) were purchased from Sigma-Aldrich. All commercial products were used as received.

PSC Growth

To synthesize MAI and MABr, 1 mol L⁻¹ HCl and 1 mol L⁻¹ HBr were poured into 1 mol L⁻¹ methylamine ethanol solution. Powder-like MAI and MABr were obtained after drying in vacuum at 150°C. To prepare the precursor solutions of MAPbCl₃, 4.05 g (1 mol L⁻¹) of MAI, 16.72 g (1 mol L⁻¹) of PbCl₂, and 45 ml of DMSO were dissolved in 60 ml of DMF. To prepare the precursor solutions of MAPbBr_{2.5}Cl_{0.5}, 6.72 g (1 mol L⁻¹) MABr, 16.52 g (0.75 mol L⁻¹) of PbBr₂, and 4.17 g (0.25 mol L⁻¹) of PbCl₂ were dissolved in 60 ml of DMF. The solutions were filtered by a polytetrafluoroethylene (PTFE) filter with a 30-μm pore size. The filtrate was then transferred to a culture dish and placed on a programmable

heating station (IKA-RET control-visc). For MAPbCl₃ PSC, the temperature was first set at 45°C and raised by 0.2°C h⁻¹ until it reached 60°C. For epitaxial and pristine MAPbBr_{2.5}Cl_{0.5} PSC, the temperature was first set at 50°C and raised by 0.2°C h⁻¹ until it reached 65°C.

Device Fabrication

To fabricate epitaxial EBL photodiodes, 100-nm poly-TPD and 50-nm Au electrodes were deposited on the face of epitaxial MAPbBr_{2.5}Cl_{0.5} PSCs, and 50-nm Ag electrodes were deposited on the face of MAPbCl₃ PSCs by thermal evaporation in vacuum. For the spin-coated EBL device, 100-nm poly-TPD and a 50-nm Au electrode were deposited on one face of pristine MAPbBr_{2.5}Cl_{0.5} PSC by thermal evaporation in vacuum and 10-nm C60 and 50-nm PCBM were deposited on the opposite face by spin coating at 1,000 r min⁻¹ in 15 s. Subsequently, Ag electrodes were deposited on it by thermal evaporation in vacuum. To optimize the epitaxial PIN photodiode surface, a diamond wire with a diameter of 0.08 mm was used to remove the extra surrounding at a sawing speed of 3,000 r min⁻¹.

Measurements

XRD patterns were obtained by X'TRA (Switzerland). SEM images and EDX were obtained by Quanta 200 FEI (USA). PL (photoluminescence) patterns were obtained by Edinburgh instruments FS5 (UK). Dark current density–voltage (*J*–*V*) characteristics were measured by a Keithley 4,200 semiconductor analyzer in darkness. The response time and transmit time were measured using an Agilent oscilloscope with a Keithley 2,400 as the voltage source and a 365-nm pulsed Nd:YAG laser with 6-ns pulse width at 20 Hz as the illumination source. Responsivity spectra were measured using Zolix tunable 500-W xenon arc lamp light as the illumination source and a Keithley 4,200 semiconductor analyzer. The photocurrent in X-ray detection performance was measured by a Keithley 6,487 Pico ammeter, and the X-ray dose rate was obtained by a commercial dosimeter (FJ-347A, China). The X-ray source was provided by Nanjing Perlove Medical Equipment Company.

RESULTS AND DISCUSSION

Pristine MAPbCl₃ PSCs considered as n-type semiconductors were grown by various temperature crystallization methods. The precursor solution was heated from 45 to 60°C for 80 h to grow MAPbCl₃ PSCs (Wang et al., 2017). First, one unit in bulk of MAPbCl₃ PSCs was synthesized by low-cost solution processes, as shown in **Figure 1A**. Then, it was placed into the precursor solution of MAPbBr_{2.5}Cl_{0.5} to induce liquid-phase epitaxial growth, in which the solution was heated from 50 to 65°C for 100 h. The MAPbBr_{2.5}Cl_{0.5} PSC slowly grew on the top and side of MAPbCl₃ in the precursor solution. Finally, the heterojunction PSC could be extracted from the solution with MAPbBr_{2.5}Cl_{0.5} enfolding MAPbCl₃ PSC as shown in **Figure 1B**. In order to fabricate the PIN photodiode, p-type poly-TPD thin film was deposited on the surface of the MAPbBr_{2.5}Cl_{0.5} PSC.

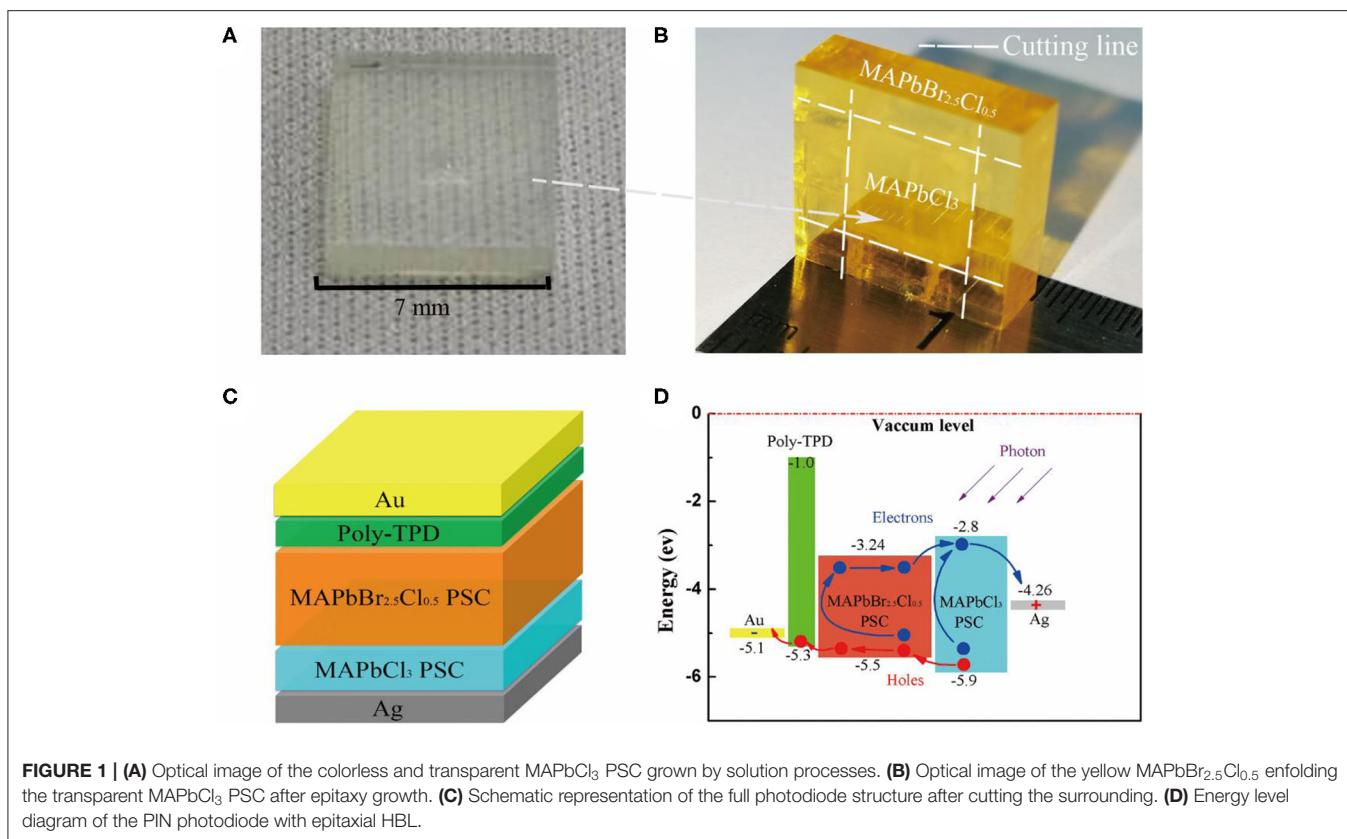
Subsequently, Au and Ag thin film was deposited on the poly-TPD layer and the surface of MAPbCl₃ PSC sequentially by thermal evaporation in vacuum.

Figure 1C shows the structure of the fabricated PIN photodiodes after cutting the surrounding, which is Au/poly-TPD/MAPbBr_{2.5}Cl_{0.5} PSC/MAPbCl₃ PSC/Ag. Poly-TPD serves as both HTL and EBL. MAPbCl₃ PSC serves as both ETL and HBL (Sutherland and Sargent, 2016). Au and Ag function as the anode and cathode, respectively. The schematic energy level diagram of the PIN photodiode is shown in **Figure 1D**, in which the photo-generated electrons and holes in the active layer are effectively separated and transported to their corresponding electrodes under external electric field. Meanwhile, poly-TPD and MAPbCl₃ PSC can effectively block the injected electrons and holes from the applied voltage source, respectively, benefiting the reduction of the dark current. The energy barriers of 4.1 eV and 1.64 eV between Au and poly-TPD and between MAPbCl₃ PSC and Ag significantly reduce the injection of electrons and holes from the anode and cathode, respectively. The energy offset between poly-TPD and the conduction band minimum (CBM) of MAPbBr_{2.5}Cl_{0.5} PSC is sufficiently large to block the transfer of electrons from MAPbBr₃ PSC to the cathode.

To optimize the crystal surface, we utilized a diamond wire to saw off the extra surrounding of the MAPbBr_{2.5}Cl_{0.5}/MAPbCl₃ heterojunction PSC bulk along the cutting lines shown in **Figure 1B**. The optical photograph of our PIN photodiode after machining the surrounding is shown in **Figure 2A**. The dimensions of our PIN photodiode are 7.28, 6.92, and 5.32 mm in length, width, and thickness, respectively. The effective electrode contact area is approximately (4.17 × 5.26 mm) 21.93 mm². Moreover, the thicknesses of the MAPbBr_{2.5}Cl_{0.5} intrinsic layer and MAPbCl₃ HBL are approximately 2.41 and 2.91 mm, respectively.

In this study, we have utilized energy dispersive X-ray (EDX) spectroscopy to investigate the lead and halide element distribution of MAPbCl₃ PSC on epitaxial MAPbBr_{2.5}Cl_{0.5}. **Figure 2B** shows the cross-sectional scanning electron micrograph (SEM) image of the epitaxial perovskite bulk. Two parts of different halide content in the bulk are selected to analyze the EDX spectra. The EDX spectra of the epitaxial MAPbBr_{2.5}Cl_{0.5} (areas outlined in yellow) and MAPbCl₃ (areas outlined in red) are shown in **Figures 2C,D**, respectively. The ratios of the Pb, Br, and Cl elements in the two kinds of perovskite layers reveal a slight difference in the ratios of the precursor solution. This can be attributed to the considerable difference in the solubility of MABr/Cl and PbBr₂/Cl₂ in DMF (Wei et al., 2016).

The comparison between X-ray diffraction (XRD) patterns of MAPbCl₃ PSC, MAPbBr_{2.5}Cl_{0.5} PSC, and MAPbCl₃ PSC on epitaxial MAPbBr_{2.5}Cl_{0.5} are shown in **Figure 3A**. From the figure, the XRD spectra of the MAPbCl₃ PSC on epitaxial MAPbBr_{2.5}Cl_{0.5} is similar to the MAPbBr_{2.5}Cl_{0.5} PSC but shifts slightly to larger angles, due to the combination of MAPbCl₃ and MAPbBr_{2.5}Cl_{0.5}. The diffraction peaks in the XRD spectra correspond to the integer of the wavelength, which indicated the one crystalline structure of MAPbCl₃.



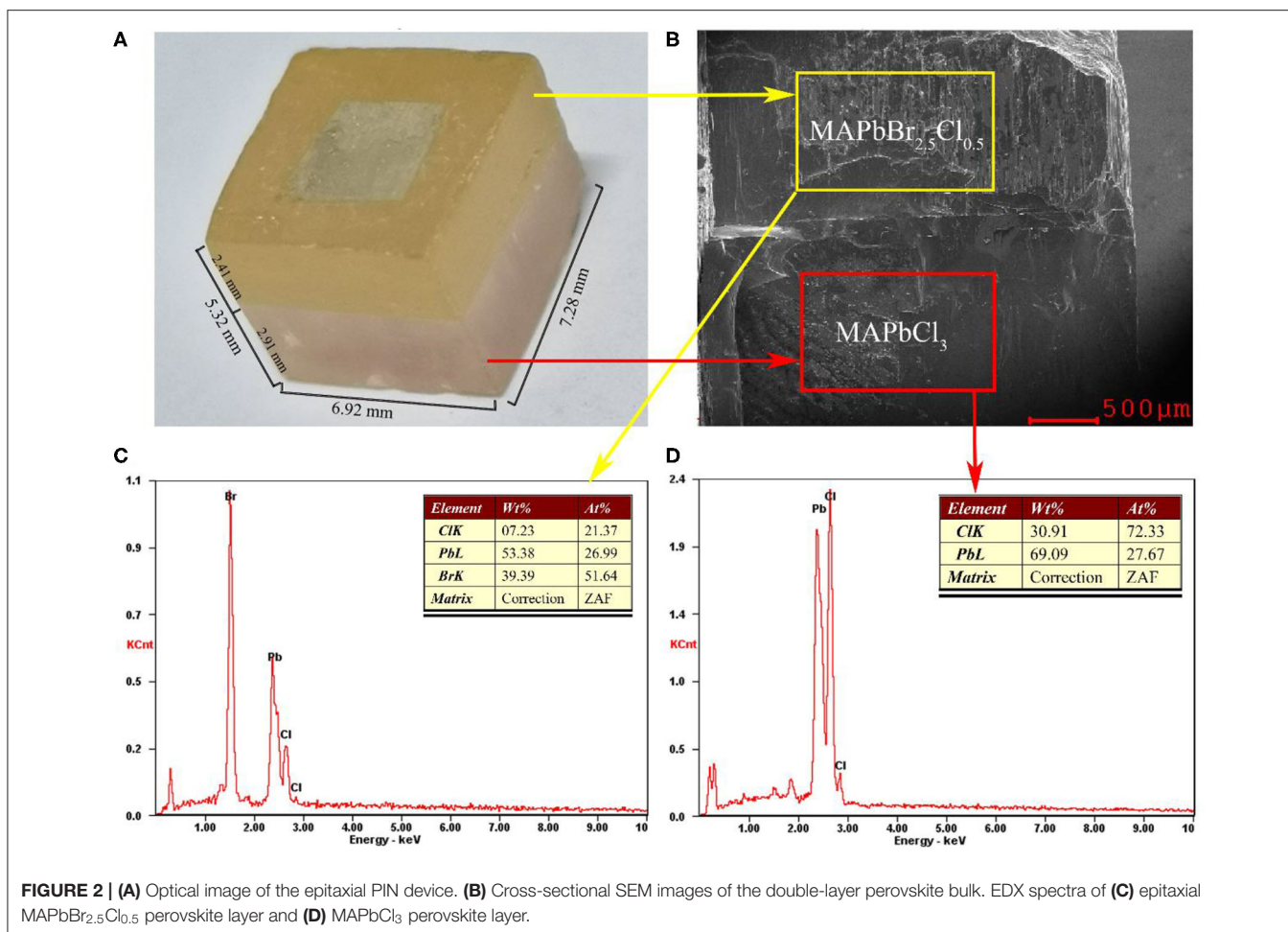
PSC on epitaxial MAPbBr_{2.5}Cl_{0.5}. The series of distinct characteristic peaks and small full width at half-maximum of the MAPbCl₃ PSC on epitaxial MAPbBr_{2.5}Cl_{0.5} indicate the high-quality crystallization. In addition, its diffraction peak positions nearly overlap with MAPbBr_{2.5}Cl_{0.5} PSC and MAPbCl₃ PSC, which corresponds to the reported graded heterojunction (Li et al., 2019b). The existence of main and secondary peaks in the XRD spectra of MAPbCl₃ PSC on epitaxial MAPbBr_{2.5}Cl_{0.5} is attributed to the diffraction of both thin epitaxial MAPbBr_{2.5}Cl_{0.5} layer and MAPbCl₃ layer.

The photoluminescence (PL) spectra of MAPbCl₃ PSC, MAPbBr_{2.5}Cl_{0.5} PSC, and epitaxial MAPbBr_{2.5}Cl_{0.5} on MAPbCl₃ block are displayed in **Figure 3B**. A 360-nm laser beam is used as the light source and incident on the surface of MAPbCl₃ PSC, MAPbBr_{2.5}Cl_{0.5} PSC, and the interface of the MAPbBr_{2.5}Cl_{0.5}-MAPbCl₃ heterojunction. The PL peaks of MAPbCl₃ PSC on epitaxial MAPbBr_{2.5}Cl_{0.5} are similar to the stack of MAPbCl₃ PSC and MAPbBr_{2.5}Cl_{0.5} PSC. From this evidence, it can hereby be concluded that the MAPbBr_{2.5}Cl_{0.5} PSC was successfully grown on the MAPbCl₃ PSC.

To show the effects of reducing lattice mismatch between heterojunction interface by epitaxially combining another kind of PSC and the enhancement of the epitaxial PIN device performance, the spin-coating device with structure Au/poly-TPD/MAPbBr_{2.5}Cl_{0.5} PSC/C60/PCBM/Ag was also fabricated for comparison.

The dark current density–voltage (J – V) characteristic curves of the epitaxial HBL device and spin-coated HBL device are shown in **Figure 4A** for comparison. The result indicates that the epitaxial HBL device shows lower dark current density than spin-coated HBL device in reverse voltage. At -250 V, the spin-coated device has a dark current density of $25 \mu\text{A cm}^{-2}$, which is only $2.9 \mu\text{A cm}^{-2}$ for the epitaxial HBL device. This indicates that the combination between the intrinsic layer and HBL by epitaxial growth contributes to the reduction of dark current. Furthermore, the dark current density of the epitaxial HBL device shows a value $<100 \text{ nA cm}^{-2}$ under -20 V, implying that the device has an advantage in the low dark current noise and large dynamic range.

Figure 4B shows the long-term dark current stability of the epitaxial HBL device and spin-coated HBL device under -250 V reverse bias voltage. As shown in the figure, the dark current of the spin-coated HBL device declines quickly in 30 s after startup and takes place at relatively high amplitude fluctuations than the epitaxial HBL device, because the spin-coated organic molecular material is unstable under a high voltage. The amplitude of the vibrated dark current for the epitaxial HBL device is $<40 \text{ nA cm}^{-2}$ but more than $4 \mu\text{A cm}^{-2}$ for the spin-coated HBL device after 2 min. The more stable long-term dark current for the epitaxial HBL device can be attributed to the better lattice matched interface between the epitaxial HBL and MAPbBr_{2.5}Cl_{0.5} PSC.



The photon detection performance is measured by a temporal photocurrent at -50 V, -100 V, -150 V, -200 V, -250 V, and -300 V, on 460-nm and 130- μ W blue light illumination, as shown in **Figures 4C,D**. All the photo responses of the epitaxial HBL device are greater than the spin-coated HBL device under different bias voltages. The rise of the photo response rate is higher than dark currents for the epitaxial HBL device with increasing bias voltage. The responsivities of the epitaxial HBL device are calculated as:

$$R = (I_{photo} - I_{dark})/P, \quad (1)$$

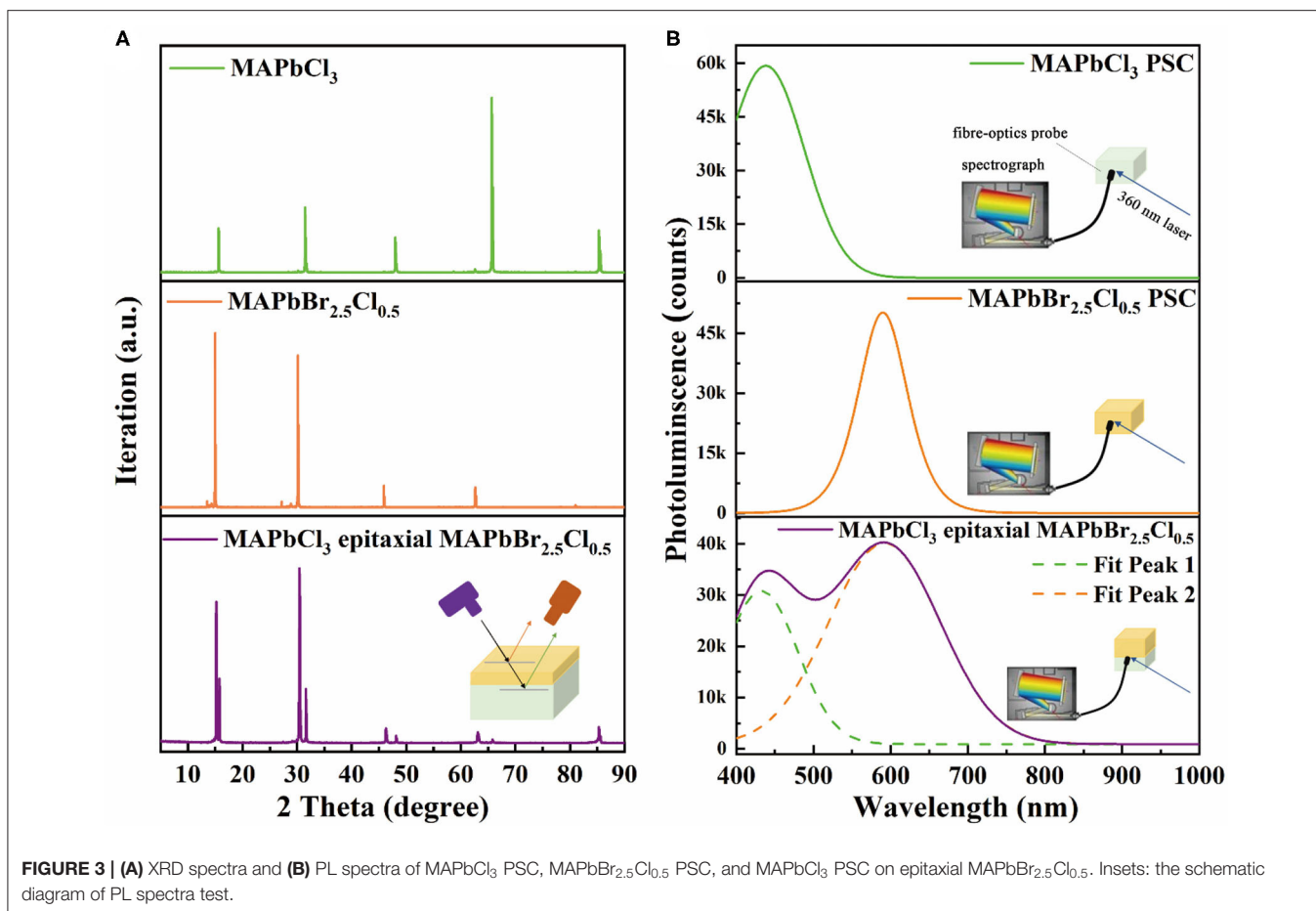
where P is incident optical power, which is 58.7 mA W⁻¹, 81.7 mA W⁻¹, 98.6 mA W⁻¹, 112 mA W⁻¹, 117 mA W⁻¹, and 122 mA W⁻¹ from -50 to -300 V, respectively. The larger responsivity is caused by the decrease of carrier recombination on the MAPbCl₃/MAPbBr_{2.5}Cl_{0.5} heterojunction interface.

Response speed is a significant factor for photodiodes that are applied in detection and imaging. In this study, a 365-nm pulsed laser with 7 ns pulse width at 20 Hz frequency is used as an excitation light source to measure the decay process of the photocurrent that reflects the detection speed of the device. **Figures 5A,B** show the decay process of the photodiodes with

epitaxial HBL and spin-coated HBL, having 5.3 and 3.2 mm thickness, respectively, under -250 V bias. The fall time defined as decaying to e^{-1} of the maximum for different devices are measured as 10 and 15 μ s, respectively, which signify that the photodiode with epitaxial HBL has a faster detection speed. Subsequently, the carrier mobilities of the epitaxial HBL and spin-coated devices are measured using the time of flight (TOF) technique. The average charge-carrier mobilities of the epitaxial HBL and spin-coated HBL devices are measured by the 365-nm nanosecond laser illuminated from the Au electrode side. The transient time for electron carrier transport through the whole perovskite device was used for average electron mobility calculation according to the formulation (Wei et al., 2016; Thirimanne et al., 2018; Hu et al., 2020):

$$\mu = d^2/V\tau, \quad (2)$$

where μ is the mobility, d is the thickness of the device, τ is the transmit time, and V is the bias voltage. The transient photocurrent responses of the epitaxial device and spin-coated device under different bias voltages were recorded and are shown in **Figures 5C,D**. By fitting the plot of τ - V^{-1} , as shown in the insets, the calculated results reveal that the



average electron mobility of the spin-coated HBL device is $188 \text{ cm}^2 \text{ V}^{-1} \text{ s}^{-1}$ while that of the epitaxial HBL device is $386 \text{ cm}^2 \text{ V}^{-1} \text{ s}^{-1}$. The epitaxial HBL device has better average electron mobility than the spin-coated HBL device, which is attributed to the substitution low surface trap single crystals for additional solution-processed layers. A detailed comparison of our epitaxial HBL perovskite photodetector with the reported layered perovskite-based photodetectors is summarized in **Table 1**.

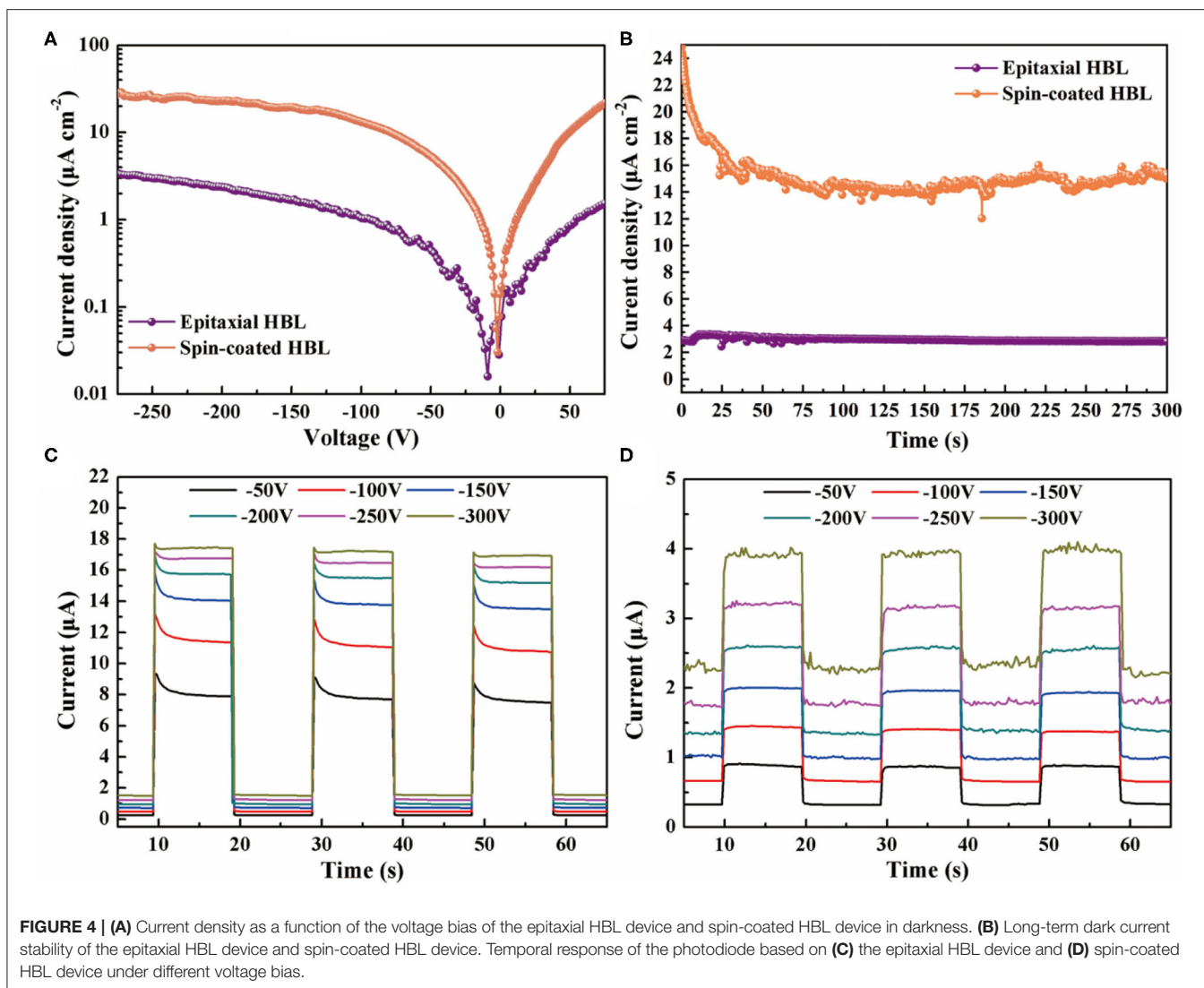
Furthermore, other key parameters of our epitaxial photodiode were also measured. When light beam with wavelength that varies continuously is incident on the cathode of the photodiode with epitaxial HBL, its responsivity spectra under different voltages are shown in **Figure 6A**. The results show a few smaller responsivity than that of temporal response in **Figure 4C** because incident light was partially obscured by the thick Ag electrode. The photodiode is most sensitive at 430 and 500 nm but almost insensitive for photons with wavelength exceeding 540 nm. With the increase of reverse voltage, the responsivity improves significantly. This is due to the different band gap for MAPbCl₃ PSC and MAPbBr_{2.5}Cl_{0.5} PSC, i.e., 3.1 and 2.26 eV, respectively. In addition, short-wave photons generate a higher current response (2.26 mA W^{-1} at 430 nm, 1.54 mA W^{-1} at 510 nm) under low-bias voltage (-10 V). However, long-wave

photons generate a higher current response (12.24 mA W^{-1} at 430 nm, 16.73 mA W^{-1} at 500 nm) under high-bias voltage (-100 V). This is because electron-hole pairs are generated at a deeper depth inside the active layer with the increase of the incident photon wavelength. Electron-hole pairs at different depths have been collected by applying different reverse voltages. The collection efficiency has also been improved with increase of the applying voltage. The noise current (I_n) of the epitaxial device under -100 V is measured as $1.12 \times 10^{-10} \text{ A Hz}^{-1/2}$ approximately. Based on the I_n and R , the specific detectivity (D^*) of the epitaxial device could be obtained by the following equations (Li et al., 2020):

$$D^* = R \times \sqrt{A f} / I_n, \quad (3)$$

where A is the active layer area and f is the bandwidth. The results of D^* value is similar to the trend of R (Li et al., 2019a). The maximum D^* of the epitaxial device is calculated about $7.32 \times 10^7 \text{ cm Hz}^{1/2} \text{ W}^{-1}$ at 500 nm under -100 V . The external quantum efficiency (EQE) of the epitaxial device under -100 V at 500 nm is calculated as about 4.5% by the following equations:

$$EQE = R \times hc / q \lambda, \quad (4)$$



where h is Plank's constant, c is the velocity of light, q is the absolute value of the electron charge, and λ is the light wavelength.

Due to the thickness of the epitaxial photodiode in the solution process being suitable for the potential application of X-ray detection, the X-ray detection performance under zero bias is also investigated in this work. Photocurrents caused by 40-keV, 60-keV, and 80-keV X-ray photons with a dose rate $27.91 \mu\text{Gy}_{\text{air}} \text{s}^{-1}$, $62.03 \mu\text{Gy}_{\text{air}} \text{s}^{-1}$, and $84.89 \mu\text{Gy}_{\text{air}} \text{s}^{-1}$, respectively, are shown in **Figure 6B**. The 5.32-mm-thick device with epitaxial EBL with self-powered shows a satisfactory response to the 40-keV, 60-keV, and 80-keV X-ray photons due to the built-in electric field of the PIN device. The X-ray detection sensitivities (S) of the epitaxial HBL device are calculated as:

$$S=Q/AX, \quad (5)$$

where Q is the collected photo charge, A is the effective detection area, and X is the radiation dose, which is $7.08 \times 10^3 \mu\text{C}$

$\mu\text{C Gy}_{\text{air}}^{-1} \text{cm}^{-2}$, $4.04 \times 10^3 \mu\text{C Gy}_{\text{air}}^{-1} \text{cm}^{-2}$, and $2.38 \times 10^3 \mu\text{C Gy}_{\text{air}}^{-1} \text{cm}^{-2}$ for the 40-, 60-, and 80-keV X-ray photons, respectively. The sensitivity of our epitaxial device with self-powered is superior to the majority of hybrid perovskite film and single crystalline device, such as MAPbI_3 film device ($25 \mu\text{C Gy}_{\text{air}}^{-1} \text{cm}^{-2}$) (Yakunin et al., 2015), CsPbBr_3 thick film device ($0.27\text{--}1.7 \times 10^3 \mu\text{C Gy}_{\text{air}}^{-1} \text{cm}^{-2}$) (Gou et al., 2019), and MAPbBr_3 single crystalline device ($80 \mu\text{C Gy}_{\text{air}}^{-1} \text{cm}^{-2}$) (Wei et al., 2016). Moreover, the sensitivity of our epitaxial device with self-powered is stronger than that of the currently commercial detectors such as a-Se, CdZnTe, HgI_2 , and PbI_2 working at a much higher field (Schieber et al., 2001). The results reveal the advantage of the application of our epitaxial PIN photodiode for X-ray detection.

CONCLUSION

To summarize, heterojunction bulk PSC has been fabricated based on liquid-phase epitaxial $\text{MAPbBr}_{2.5}\text{Cl}_{0.5}$ on MAPbCl_3

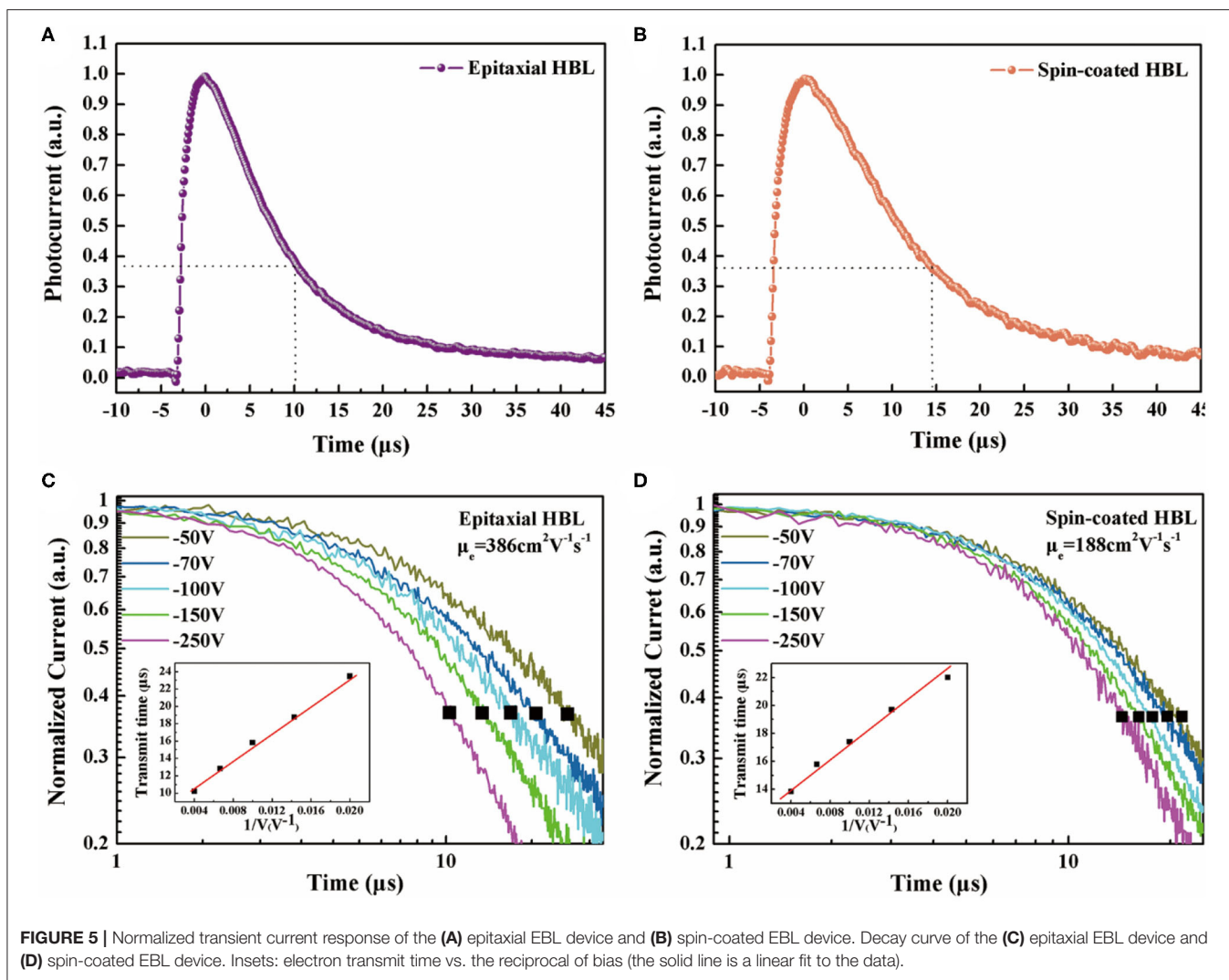
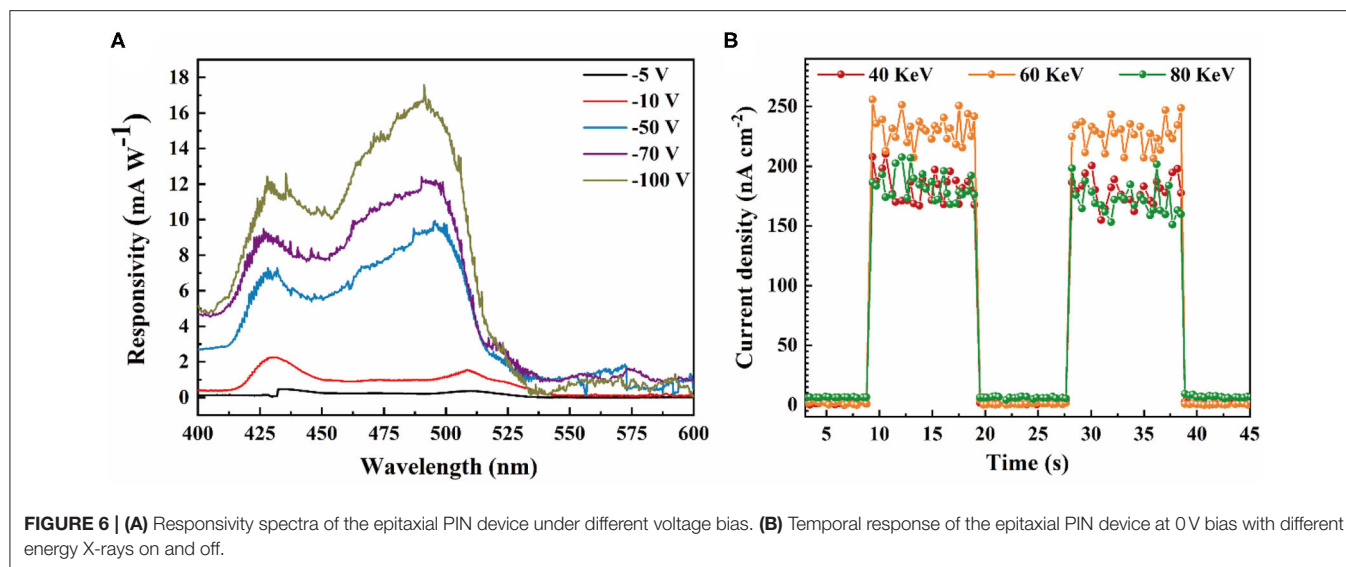


TABLE 1 | Comparison of the epitaxial HBL perovskite photodetector with the reported layered perovskite photodetectors.

Device structure	Responsivity (mA W^{-1}) @ applied electric field, light source	Decay time (μs) @ applied electric field	References
Au/poly-TPD/MAPbBr ₃ PSC/C60 doped PCBM/Ag	1.252 @ 0.003 V/ μm , 532 nm light	26 @ 0.015 V/ μm	Wang et al., 2018
Glass/SnO ₂ /PCBM/MAPbI ₃ /Au	11.8 @ 0.05 V/ μm , 460 nm light	63.3 @ 0.05 V/ μm	Su et al., 2019
FTO/TiO ₂ /MAPbI ₃ /PDCBT or Spiro-OMeTAD/Au	92 @ 0 V/ μm , 405 nm light 132 @ 0.3 V/ μm , 620 nm light	210 @ 0 V/ μm 140 @ 0.3 V/ μm	Tang et al., 2019
ITO/MAPbI ₃ /PCBM/C60/Ag	35 @ 0.066 V/ μm , white light	227 @ 0.066 V/ μm	Lv et al., 2018
Au/poly-TPD/MAPbBr _{2.5} Cl _{0.5} -MAPbCl ₃ /Ag	117 @ 0.047 V/ μm , 460 nm light	10 @ 0.047 V/ μm	This study

PSC. A 10-fold reduction of the dark current is achieved for the PIN photodiode with epitaxial HBL in comparison to the photodiode fabricated by spin-coated additional organic n-type semiconductor materials as HBL. Additionally, the epitaxial HBL device also shows greater responsivity, better stability, faster response time to 10 μs , and a higher average charge-carrier mobility up to 386 $\text{cm}^2 \text{V}^{-1} \text{s}^{-1}$ than the

spin-coated HBL device. The device also reveals a satisfactory detection sensitivity up to several $\text{mC Gy}_{\text{air}}^{-1} \text{cm}^{-2}$ for 40- to 80-keV X-ray photons. This research proves that epitaxial growth is a more reliable, effective method to fabricate perovskite-perovskite heterojunctions and can avoid lattice mismatch on the interface. Hence, the use of epitaxial PSC HBL to form heterojunction interface can be a promising



method for the fabrication of high-performance perovskite photodiode devices.

DATA AVAILABILITY STATEMENT

The raw data supporting the conclusions of this article will be made available by the authors, without undue reservation.

AUTHOR CONTRIBUTIONS

YP, XW, and YX grew the perovskite single crystals. YP conducted the epitaxial experiments and wrote this manuscript.

YP and YL conducted the measurements. XW and YP analyzed the results. All authors have made comments on the manuscript.

FUNDING

This work was supported by the National Key R&D Program of China (Grant Nos. 2017YFC0111500 and 2016YFB0401600), the National Natural Science Foundation Project (Grant Nos. 61775034, 61571124, and 61674029), and the International Cooperation Program of Jiangsu Province (Grant No. BZZ2018056).

REFERENCES

- Chen, Z., Du, X., Zeng, Q., and Yang, B. (2017). Recent development and understanding of polymer-nanocrystal hybrid solar cells. *Mater. Chem. Front.* 1, 1502–1513. doi: 10.1039/C7QM00022G
- Cheng, X., Yang, S., Cao, B., Tao, X., and Chen, Z. (2019). Single crystal perovskite solar cells: development and perspectives. *Adv. Funct. Mater.* 30:1905021. doi: 10.1002/adfm.201905021
- Dai, X., Zhang, Z., Jin, Y., Niu, Y., Cao, H., Liang, X., et al. (2014). Solution-processed, high-performance light-emitting diodes based on quantum dots. *Nature* 515, 96–99. doi: 10.1038/nature13829
- Fang, Y., and Huang, J. (2015). Resolving Weak Light of Sub-picowatt per Square Centimeter by Hybrid Perovskite Photodetectors Enabled by Noise Reduction. *Adv. Mater.* 27, 2804–2810. doi: 10.1002/adma.201500099
- Gill, H. S., Elshahat, B., Kokil, A., Li, L., Mosurkal, R., Zygmanski, P., et al. (2018). Flexible perovskite based X-ray detectors for dose monitoring in medical imaging applications. *Phys. Med.* 5, 20–23. doi: 10.1016/j.phmed.2018.04.001
- Gou, Z., Huanglong, S., Ke, W., Sun, H., Tian, H., Gao, X., et al. (2019). Self-powered X-ray detector based on all-inorganic perovskite thick film with high sensitivity under low dose rate. *Phys. Status Solidi Rapid Res. Letters* 13:1900094. doi: 10.1002/pssr.201900094
- Hu, M., Jia, S., Liu, Y., Cui, J., Zhang, Y., Su, H., et al. (2020). Large and dense organic-inorganic hybrid perovskite CH₃NH₃PbI₃ wafer fabricated by one-step reactive direct wafer production with high x-ray sensitivity. *ACS Appl. Mater. Interfaces* 12, 16592–16600. doi: 10.1021/acsami.9b23158
- Jara, D. H., Yoon, S. J., Stamplecoskie, K. G., and Kamat, P. V. (2014). Size-dependent photovoltaic performance of CuInS₂ quantum dot-sensitized solar cells. *Chem. Mater.* 26, 7221–7228. doi: 10.1021/cm5040886
- Jiang, S., Wang, X., Wu, Y., Li, Y., Zhang, Q., Li, G., et al. (2019). Balance lead in solution-processed CH₃NH₃PbBr_xCl_(3-x) single crystals for high performance X-ray detection. *Mater. Lett.* 236, 26–29. doi: 10.1016/j.matlet.2018.10.055
- Ju, M.-G., Chen, M., Zhou, Y., Dai, J., Ma, L., Padture, N. P., et al. (2018). Toward eco-friendly and stable perovskite materials for photovoltaics. *Joule* 2, 1231–1241. doi: 10.1016/j.joule.2018.04.026
- Kojima, A., Miyasaka, T., Teshima, K., and Shirai, Y. (2009). Organometal halide perovskites as visible-light sensitizers for photovoltaic cells. *J. Am. Chem. Soc.* 131, 6050–6051. doi: 10.1021/ja809598r
- Li, C., Lu, J., Zhao, Y., Sun, L., Wang, G., Ma, Y., et al. (2019a). Highly sensitive, fast response perovskite photodetectors demonstrated in weak light detection circuit and visible light communication system. *Small* 15:e1903599. doi: 10.1002/smll.201903599
- Li, C., Wang, H., Wang, F., Li, T., Xu, M., Wang, H., et al. (2020). Ultrafast and broadband photodetectors based on a perovskite/organic bulk heterojunction for large-dynamic-range imaging. *Light Sci. Appl.* 9:31. doi: 10.1038/s41377-020-0264-5
- Li, W.-G., Wang, X.-D., Liao, J.-F., Wei, Z.-F., Xu, Y.-F., Chen, H.-Y., et al. (2019b). A laminar MAPbBr₃/MAPbBr_{3-x}I_x graded heterojunction single crystal for enhancing charge extraction and optoelectronic performance. *J. Mater. Chem. C* 7, 5670–5676. doi: 10.1039/C9TC00972H

- Lin, Q., Armin, A., Lyons, D. M., Burn, P. L., and Meredith, P. (2015). Low noise, IR-blind organohalide perovskite photodiodes for visible light detection and imaging. *Adv. Mater.* 27, 2060–2064. doi: 10.1002/adma.201405171
- Liu, D., and Kelly, T. L. (2014). Perovskite solar cells with a planar heterojunction structure prepared using room-temperature solution processing techniques. *Nat. Photonics* 8, 133–138. doi: 10.1038/nphoton.2013.342
- Lv, Q., Lian, Z., He, W., Sun, J.-L., Li, Q., and Yan, Q. (2018). A universal top-down approach toward thickness-controllable perovskite single-crystalline thin films. *J. Mater. Chem. C* 6, 4464–4470. doi: 10.1039/C8TC00842F
- Malinkiewicz, O., Yella, A., Lee, Y. H., Espallargas, G. M., n., Graetzel, M., et al. (2014). Perovskite solar cells employing organic charge-transport layers. *Nat. Photonics* 8, 128–132. doi: 10.1038/nphoton.2013.341
- Ou, Q., Bao, X., Zhang, Y., Shao, H., Xing, G., Li, X., et al. (2019). Band structure engineering in metal halide perovskite nanostructures for optoelectronic applications. *Nano Mater. Sci.* 1, 268–287. doi: 10.1016/j.nanoms.2019.10.004
- Schieber, M., Hermon, H., Zuck, A., Vilensky, A., Melekhov, L., Shatunovsky, R., et al. (2001). Thick films of X-ray polycrystalline mercuric iodide detectors. *J. Crystal Growth* 225, 118–123. doi: 10.1016/S0022-0248(01)00832-6
- Su, H., Meng, L., Liu, Y., Zhang, Y., Hu, M., Yang, Z., et al. (2019). Effective electron extraction from active layer for enhanced photodetection of photoconductive type detector with structure of Au/CH₃NH₃PbI₃/Au. *Org. Electron* 74, 197–203. doi: 10.1016/j.orgel.2019.06.015
- Sutherland, B. R., and Sargent, E. H. (2016). Perovskite photonic sources. *Nat. Photonics* 10, 295–302. doi: 10.1038/nphoton.2016.62
- Tan, Z.-K., Moghaddam, R. S., Lai, M. L., Docampo, P., Higler, R., Deschler, F., et al. (2014). Bright light-emitting diodes based on organometal halide perovskite. *Nat. Nanotechnol.* 9, 687–692. doi: 10.1038/nnano.2014.149
- Tang, X. F., Matt, G. J., Gao, S., Gu, E., Almora, O., and Brabec, C. J. (2019). Electrical-field-driven tunable spectral responses in a broadband-absorbing perovskite photodiode. *ACS Appl. Mater. Interfaces* 11, 39018–39025. doi: 10.1021/acsami.9b14788
- Thirimanne, H. M., Jayawardena, K., Parnell, A. J., Bandara, R. M. I., Karalasingam, A., Pani, S., et al. (2018). High sensitivity organic inorganic hybrid X-ray detectors with direct transduction and broadband response. *Nat. Commun.* 9, 2926. doi: 10.1038/s41467-018-05301-6
- Wang, H., and Kim, D. H. (2017). Perovskite-based photodetectors: materials and devices. *Chem. Soc. Rev.* 46, 5204–5236. doi: 10.1039/C6CS00896H
- Wang, J., Wang, N., Jin, Y., Si, J., Tan, Z.-K., Du, H., et al. (2015). Interfacial control toward efficient and low-voltage perovskite light-emitting diodes. *Adv. Mater.* 27:2311. doi: 10.1002/adma.201405217
- Wang, X., Huang, Y., Lei, W., Li, Q., Zhang, X., Khan, Q., et al. (2017). Asymmetrical photodetection response of methylammonium lead bromide perovskite single crystal. *Crystal Res. Technol.* 52:5. doi: 10.1002/crat.201700115
- Wang, X., Wu, Y., Li, G., Li, Y., Wu, J., Zhang, X., et al. (2019). Fabrication of photodiodes based on solution-processed perovskite single crystals. *IEEE Trans. Electron Devices* 66, 485–490. doi: 10.1109/TED.2018.2878828
- Wang, X., Zhao, D., Qiu, Y., Huang, Y., Wu, Y., Li, G., et al. (2018). PIN diodes array made of perovskite single crystal for X-ray imaging. *Phys. Status Solidi Rapid Res. Letters* 12:7. doi: 10.1002/pssr.201800380
- Wei, H., Fang, Y., Mulligan, P., Chuirazzi, W., Fang, H.-H., Wang, C., et al. (2016). Sensitive X-ray detectors made of methylammonium lead tribromide perovskite single crystals. *Nat. Photonics* 10, 333–339. doi: 10.1038/nphoton.2016.41
- Yakunin, S., Sytnyk, M., Kriegner, D., Shrestha, S., Richter, M., Matt, G. J., et al. (2015). *Detection of X-Ray Photons by Solution-Processed Lead Halide Perovskites*. Great Britain: Nature Publishing Group. doi: 10.1038/nphoton.2015.82
- Zeng, X., Zhou, T., Leng, C., Zang, Z., Wang, M., Hu, W., et al. (2017). Performance improvement of perovskite solar cells by employing a CdSe quantum dot/PCBM composite as an electron transport layer. *J. Mater. Chem. A* 5, 17499–17505. doi: 10.1039/C7TA00203C
- Zhang, Y., Yuan, Y., and Huang, J. (2017). Detecting 100 fW cm⁻² light with trapped electron gated organic phototransistors. *Adv. Mater.* 29:1603969. doi: 10.1002/adma.201603969

Conflict of Interest: The authors declare that the research was conducted in the absence of any commercial or financial relationships that could be construed as a potential conflict of interest.

Copyright © 2020 Pan, Wang, Xu, Li, Elemike, Shuja, Li, Zhang, Chen, Zhao and Lei. This is an open-access article distributed under the terms of the Creative Commons Attribution License (CC BY). The use, distribution or reproduction in other forums is permitted, provided the original author(s) and the copyright owner(s) are credited and that the original publication in this journal is cited, in accordance with accepted academic practice. No use, distribution or reproduction is permitted which does not comply with these terms.